24

Tailoring of Morphology and Mechanical Properties of Isotactic Polypropylene by Processing

K. Schneider[1], L. Häussler[1] and S.V. Roth[2]
[1]*Leibniz-Institut für Polymerforschung Dresden,*
[2]*DESY, Hamburg,*
Germany

1. Introduction

The deformation behaviour of semi-crystalline materials is mainly determined by the behaviour of the two components – the crystalline and the amorphous phase with their characteristic temperature-dependent mechanical behaviour and sometimes their anisotropy. So the crystalline phase is elastically with a rather high modulus. Above a certain stress the crystallites break down into smaller fragments. Aligned chains enable recrystallisation. The mobility in the amorphous phase depends on the difference between the ambient temperature and the temperature characteristic of the glass transition, which is the dominant relaxation process in the temperature range under investigation. On the other side the amorphous phase is constrained within the crystalline one. So it shows to some extent stress relaxation or frozen stress. Both phases are connected via anchor molecules, bridging the phase boundaries. Those molecules are mainly responsible for stress transfer between the phases.

The actual morphology and so the subsequent interaction of the different phases within a samples are mainly determined by processing and the thermal history of the material. For instance, in an injection moulded plate the properties can be extremely dependent on the position and direction of a specimen, changing from relatively brittle to highly stretchable (Schneider, 2010).

The whole stress-strain curves of semi-crystalline materials generally show three characteristic regions. Although the initial region prior to the yield point apparently behaves elastically, stress relaxation due to rearrangements in the amorphous phase can be observed also here. The mobility in the amorphous phase depends on the difference between the ambient temperature and the temperature characteristic of the glass transition, which is the dominant relaxation process in the temperature range under investigation. In the case of confined stretched amorphous regions between crystalline phases the glass transition temperature can be changed significantly. After the yield point typically local necking occurs with high local strain while the overall strain remains moderate. In the case of dog-bone specimens then the neck propagates over the whole specimen during constant load. In the true stress-strain diagram necking is a fast local deformation from the yield strain to the

strain of the fully yielded specimen. In the third step during further elongation strain hardening occurs, until finally the specimen fails. Here the strain hardening modulus can be a relevant parameter for the long term stability against creep (Kurelec, 2005).

Already in his first model of structural changes during deformation Peterlin (Peterlin, 1971) discussed spherulites consisting of lamellae separated by amorphous regions. Due to tie molecules stress is transferred between the lamellae inducing deformation and finally disintegration and rearrangement in the form of fibrillae. Later numerous authors modified and enhanced Peterlin's approach to describe their experiments. The discussion gained new impetus after the first online structure investigation during deformation by Zuo et al. (Zuo, 2005).

Breese and Beaucage (Breese, 2004, 2008) gave an overview of older models. Finally, they describe mechanical behaviour with a model refining the models of Weeks and Porter (Weeks, 1974) and Gibson, Davies and Ward (Gibson, 1978) in the sense that the effects of the orientation process on the modulus of the non-fibrous gel component are incorporated into the model by allowing a transition to fibres.

To describe the deformation behaviour of semi-crystalline polymers Strobl et al. (Hong, 2004, 2006) separated different mechanisms of stress transfer with respect to amorphous and crystalline units. They distinguished between four phases: onset of local block sliding (1), collective motion slightly below the yield point (2), disassociation of crystalline blocks and transformation into fibrils (3) and the start of disentangling (4).

In most models the common process of cavitation in polymers during deformation is not yet incorporated. Many systems show a characteristic whitening during plastic deformation due to the formation of voids or cavities with a typical length scale growing up to the wavelength of visible light, i.e. some hundreds of nanometres (Pawlak, 2010; Men, 2004). It is obvious that these large-scale structures are not accessible with a conventional small angle X-ray scattering setup. But at least the beginning of this process should be well detectable by X-ray scattering due to the strong difference in electron density between the polymer and the voids in the relevant angular range accessible by USAXS (Ultra-SAXS (Lode, 1998; Gehrke, 1995; Roth, 2006)).

In previous studies Davies et al. (Davies, 2004) demonstrated a continuous generation of the voids in the plastic phase starting at the yield point, which led to a conspicuous increase in the scattering power. Furthermore, a change in the diffuse scattering profile indicates a monotone change in the size and in the shape of the voids.

Stribeck et al. (Stribeck, 2008) described nanostructure evolution in Polypropylene during online mechanical testing with simultaneous SAXS and refined details of the interaction between the different phases including cavitation.

As an example the properties of isotactic Polypropylene (iPP) samples, produced by compression and injection moulding as well as after hot stretching, respectively, were investigated under stepwise loading. Simultaneously the structural changes were characterised by Synchrotron-SAXS and –WAXS and discussed together with the mechanical properties. It was found that there is a highly preoriented structure within the injection moulded specimen, which strongly influences the further temperature-dependent deformation behaviour. The influence of temperature and pre-orientation on the deformation behaviour is

described extending the present models of plastic deformation. The detailed knowledge of the structure and the microscopical behaviour of the material enables the tailoring of the processing conditions for material with certain mechanical behaviour.

Recently we published an overview about our first investigations about the structural changes in iPP during deformation using SAXS, WAXS, DSC and SEM-micrographs (Schneider, 2010, 2011). The present work will complement and round up the investigations described in those papers.

2. Experimental

2.1 General procedure

In order to investigate structural modifications during deformation X-ray scattering experiments were performed on samples mounted in a miniaturised tensile rig placed in the synchrotron X-ray beam. The synchrotron radiation is necessary to have sufficient intensity to get high time resolution. A general description of the equipment was given by Davies et al. (Davies, 2004).

The actually used experimental arrangement and the specimen geometry are illustrated in figure 1.

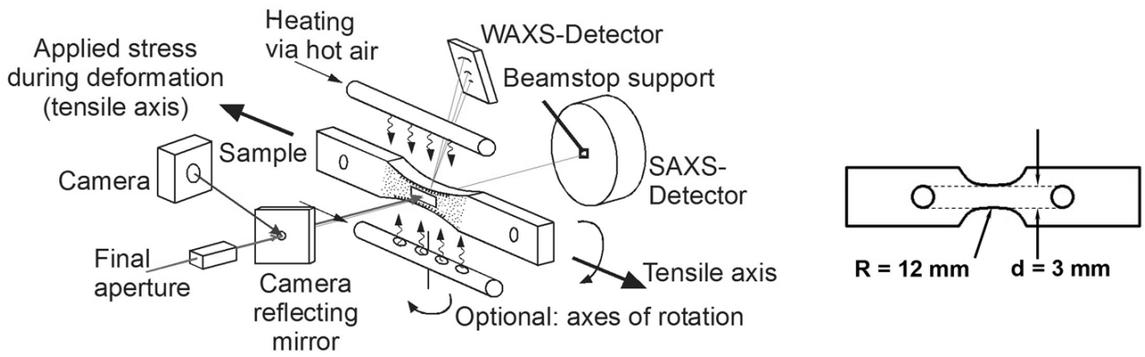

Fig. 1. Sketch of the experimental arrangement for SAXS and WAXS during deformation (left) and waisted specimen (mini-dumbbell) mainly used for simultaneous structure and mechanical investigation (right), the dimensions of the specimen can be scaled.

To investigate local strain-dependent properties, small waisted specimens were used in order to concentrate the stress in the centre of the specimen. By using a relatively large radius of curvature (12 mm) compared to the specimen width (3 mm) the stress state in the middle of the specimen is in good approximation maintained constant. The strain was determined optically by observing the deformation of a grid pattern applied on the specimen surface. The grid pattern was applied using a self-made flexible ink and a mesh size of 0.35 mm. Alternatively, also a classical image correlation analysis for strain estimation can be used. A comparison of stress-strain curves of the waisted specimens with standardised dog-bone specimens shows a good consistency: The curve progression from the beginning to the yield point as well as during strain hardening (that is where the yielded parallel region of the dog-bone specimen is deformed in a uniform way) are identical. For the range of neck formation and propagation in the dog-bone specimen an estimation of true

stress and strain via global strain measurement are not possible. Only a local strain measurement solves this problem. In the present context the specimens are approximated as incompressible. This allows us to calculate the true stress σ_t from the measured force F, initial cross section A and tensile strain ε_t as $\sigma_t = F * (1 + \varepsilon_t) / A$.

In order to keep the beam in a fixed position relative to the gauge length of the waisted sample throughout the measurement, both grips were moved simultaneously in opposite direction.

To get simultaneous SAXS and WAXS patterns, the WAXS could be monitored only in a limited range using a tilted detector. By using a horizontal tensile direction the vertically arranged WAXS detector monitors mainly the equatorial scattering of the sample. To follow also quick changes exclusively in the crystalline phase WAXS measurements were performed alternatively with the WAXS detector directly in the beam behind the sample and a sampling rate of 1 s.

For temperature-dependent tensile and scattering experiments a small heating device blows locally preheated air at the sample.

Besides the global scanning of samples the experimental setup generally also permits spatially resolved pattern recording, e. g. around a crack tip, if it is employed in a microfocus beamline. The described arrangement was successfully used investigating semi-crystalline polymers during deformation (Schneider, 2006, 2010, 2011) and fracture (Schneider, 2008, 2009).

2.2 Measurements at synchrotron beamlines

WAXS and SAXS measurements during deformation were performed at the synchrotron beamlines BW4 and P03 at HASYLAB in Hamburg, Germany (Roth, 2006). At BW4 the wavelength of the X-ray beam was 0.13808 nm, the beam diameter was about 400 µm. The SAXS images were collected by a two-dimensional MarCCD-detector (2048 x 2048 pixels of 79.1 x 79.1 µm²). The sample-to-detector distance was set to 4080 mm. The WAXS images were collected by a two-dimensional PILATUS 100K-detector (487 x 195 pixels of 172 x 172 µm²). The position of the WAXS detector was estimated using certain reference reflexes of iPP. By a special procedure the position of the tilted WAXS-detector was determined to have a tilt angle of 22.7°. The distance between the sample and the point of normal incidence was 247 mm. Exposure times were chosen in the range of 5 to 60 s per pattern. The frame rate, determined by exposure and data storage, was 15 to 70 s per pattern.

Additionally, WAXS measurements were performed at the synchrotron beamline P03 at HASYLAB (for a beamline overview see Roth et al., 2011) with a wavelength of 0.0941 nm and a beam size of about 15 µm diameter, using a PILATUS 300K-detektor (487 x 619 pixels of 172 x 172 µm²). The detector was placed vertically in the beam in a distance of 144.9 mm, the sampling rate was 1 s. To prevent sample damage due to the high intensity of the used X-ray beams at P03 during the measurements normally slow scans along or across the sample were performed.

For the discussion all SAXS- and WAXS-2D-patterns are shown with vertical tensile direction. For specimens with fibre symmetry this means that the fibre axis and so the scattering vector s_3 is also vertical, the scattering vector s_{12} is always horizontal.

2.3 Supplementary investigations of the material properties

For the investigation of the general temperature-dependent stress-strain-behaviour and the preparation of specimens for dynamic mechanical analysis (DMA) of highly stretched specimens short dogbone-specimen (parallel length 25 mm, specimen width 10 mm, thickness 4 mm, strain rate 80 mm/min) were measured with a testing machine Zwick 1456 from Zwick, Germany with heating chamber and optical strain measuring system.

DMA was performed by a rheometer ARES G2 from TA-instruments in torsion mode with a heating rate of 5 K/min and a frequency of 1 rad/s (6.28 Hz) as well with a dynamic mechanical spectrometer EPLEXOR 150N from GABO QUALIMETER Testanlagen GmbH, Germany in tensile mode with a heating rate of 3 K/min and a frequency of 1 Hz.

For qualitative comparison of crystallinity and the melting behaviour of samples stretched under certain conditions some differential scanning calorimeter (DSC) measurements were performed on drawn samples using a DSC Q 1000 from TA-instruments. The specimens were measured between -80 and 230 °C with a heating rate of 20 K/min. Before each scan the sample was equilibrated at constant temperature for 300 s. In the case of heating into the melting region a heating rate of 10 K/min and a subsequent cooling rate of 80 K/min were used.

As qualitative check of the discussed structures some SEM images of the drawn samples were taken on a Zeiss Gemini Ultra plus SEM.

2.4 Material and sample preparation

The investigations were done on isotactic polypropylene (iPP), grade HD 120 MO from Borealis. Both injection and compression moulded plates were used. The melt temperature in injection moulding was 245 °C, the mould temperature was 40 °C. The mould has a film gate with a width of the half of plates thickness.

Compression moulded plates were used, produced by heating injection moulded plates to 210 °C for 5 minutes in a vacuum press. Then the plates were cooled down to room temperature at 15 K/min. The specimen used for scattering have always a thickness of about 1 mm. Mini-dumbbell specimens were produced by CNC milling. For the investigation of the general temperature-dependent stretching behaviour from the plates with 4 mm thickness short dumbbell specimen (parallel length 25 mm, specimen width 10 mm, thickness 4 mm) were produced also by CNC milling.

3. Evaluation of scattering data

3.1 SAXS data evaluation

The evaluation of SAXS images is strongly related to the approach for materials with fibre symmetry developed by Stribeck (Stribeck, 2007). Data processing was realised with the software package pv-wave from Visual Numerics.

The images were normalised with respect to the incident flux and blind areas were masked. Considering the sample absorption the instrument background was subtracted. By translation and rotation the images were aligned in that way that the tensile direction is

vertical and the beam position in the middle of the patterns. Finally, the patterns were averaged with respect to the four quadrants of the detector. The blind area of the beam stop is interpolated assuming a Guinier-type behaviour of intensity in this range.

Generally, SAXS realises a projection of the specimen structure into the reciprocal space, where it produces a slice of the Fouriertransform (FT) of the structure whose amplitude is measured. A single back-transformation would deliver a projection of the autocorrelation function of the structure.

Complete information about the specimen would be available only by tomographic methods with a stepwise rotation of the sample (see e.g. Schroer, 2006) or using inherent symmetry properties of the sample. Under the assumption of fibre symmetry of the stretched specimen around the tensile axis, from the slices through the squared FT-structure the three-dimensional squared FT-structure in reciprocal space can be reconstructed and hence also the projection of the squared FT-structure in reciprocal space. The Fourier back-transformation of the latter delivers slices through the autocorrelation function of the initial structure. Stribeck pointed out that the chord distribution function (CDF) as Laplace transform of the autocorrelation function can be computed from the scattering intensity I(s) simply by multiplying I(s) by the factor $L(s) = -4\pi^2(s_{12}^2 + s_3^2)$ prior to the Fourier back-transformation. Here s is the scattering vector with the component s_{12} in transversal direction and s_3 in fibre direction.

The interpretation of the CDF is straightforward (Stribeck, 2001), since it has been defined by the Laplacian of Vonk's multidimensional correlation function (Vonk, 1979). It presents autocorrelations of surfaces from the scattering entities in that way that positive values characterise distances between surfaces of opposite direction, negative values distances between surfaces of the same direction, see figure 2.

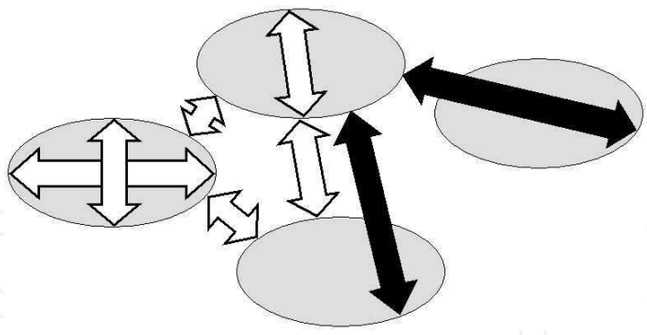

Fig. 2. Information of CDF's: In any particular structure positive values of the CDF represent correlations of interfaces with opposite direction (light arrows); negative values represent correlation of interfaces with the same direction (dark arrows).

Hence positive peaks in the vicinity of the origin characterise size distributions of the primary domains. In the case of semi-crystalline materials this can be crystallites as well as amorphous regions in-between. If cavitation occurs it will be superimposed by the size of the cavities. Also a relatively small amount of cavities will be visible because the difference in electron density is here much higher than between crystalline and amorphous phase within the polymer.

Following negative peaks characterise distances between adjacent repetition units ("long periods").

Positive peaks at greater distances describe size and orientation of domains (from the beginning of the first domain to the end of the second one). In well oriented systems also peaks of higher order can be observed.

For detailed discussion the CDF's can be presented as contour plots or as density plots in the plane.

3.2 WAXS data handling

Unfortunately, the PILATUS detector has some dark regions. After masking the beam stop those regions were reconstructed using the symmetry properties of the pattern.

For the qualitative discussion in the present case the individual images were not normalised with respect to the incident flux and not corrected with respect to background scattering.

4. Results

4.1 Mechanical behaviour of injection moulded iPP

The temperature-dependent stress-strain-behaviour of iPP is shown in figure 3.

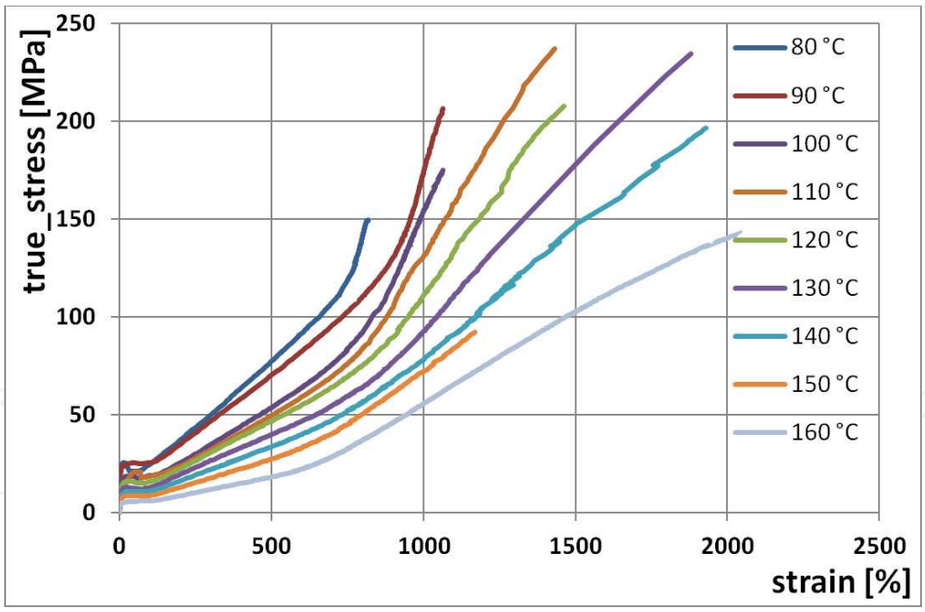

Fig. 3. Temperature-dependent stress-strain-behaviour

The general behaviour is characterized by a decrease of the initial modulus as well as the yield stress with temperature. Yielding of the material is finished at a strain of about 600 … 900 %, afterwards there is a strain hardening. The strain hardening modulus (slope of the true stress vs. strain curve in the region of strain hardening) decreases with the temperature.

The stress at failure initially increases with the temperature. At temperatures above 130 °C the stress at failure again decreases. The strain at failure increases steadily to finally more than 2000 %.

There is some whitening of the specimens, mainly due to cavitation. It starts at lower temperatures above the yielding point. With increasing temperatures the initiation of whitening shifts to higher strains. At temperatures above 110 °C it happens in the strain hardening region, with increasing temperature nearer to failure.

The small decay in the curves above the yielding point is due to the fact, that these experiments were performed with tensile bars with parallel gauge length and a distance of the optical marks of about 10 mm. Using samples with waisted geometry and strongly localized optical strain measurement this decay can be prevented to the greatest extent (Schneider, 2010).

4.2 Crystallite identification

According to Bragg's law the positions of WAXS reflexes refer to the distance between crystalline planes within the crystallites. In the compression moulded as well as in the injection moulded plates a couple of crystalline reflexes could be identified. The reflexes with the highest intensity within the relevant angular region are summarised in table 1.

Reflex	Intensity (qualitatively)	d / nm	Scattering angle 2 Θ / deg	
			P03	BW4
1 1 0	strong	0.6269	8.608	12.64
0 4 0	strong	0.5240	10.303	15.13
1 3 0	strong	0.4783	11.291	16.59
1 1 1	strong	0.4170	12.957	19.05
0 4 1	strong	0.4058	13.316	19.58

Table 1. Crystalline reflexes of iPP, which were used for the calibration of the detector distance as well as for the further discussion of crystallite orientation and changes during deformation.

4.3 Elastic crystallite deformation

Loading of the samples below the yield point causes a certain deformation of Debye-Scherrer patterns of the crystallites. According to Bragg's law a scattering signal refers to the spacing between lattice planes. The shift inversely reflects the strain vertical to the corresponding plane. In the present context the longitudinal tension as well as the transversal compression could be followed. Due to the stiffness of the crystallites deformations only in the range of about 1 % could be found, which are difficult to be resolved with the pixel size of the used detector. By unloading the samples the crystallite reflexes shift again to the initial positions. Similarly, also the thermal expansion of the crystals could be found only qualitatively.

This behaviour we reported yet in the past (Schneider, 2010), where we compared the mismatch between crystalline and global strain by a factor in the order of 10 indicating the different stiffness of the crystallites compared to that of the whole specimen due to the relatively soft amorphous regions.

In the present context the shift of the observed (h k 0)-reflexes in equatorial direction (perpendicular to tensile direction) display the transversal crystalline strain of the crystallites aligned in tensile direction.

Cyclic loading and unloading gives an estimation of the elastic crystalline strain also during plastic deformation. Figure 4 shows transversal crystalline strain of the (1 1 0)-reflex vs. the overall tensile strain for 3 consecutive loading cycles. The first strain amplitude was 0.12, the remaining strain after unloading 0.04. The following cycles were conducted within the overall elastic region. The shift of other (h k 0)-reflexes yield the same result.

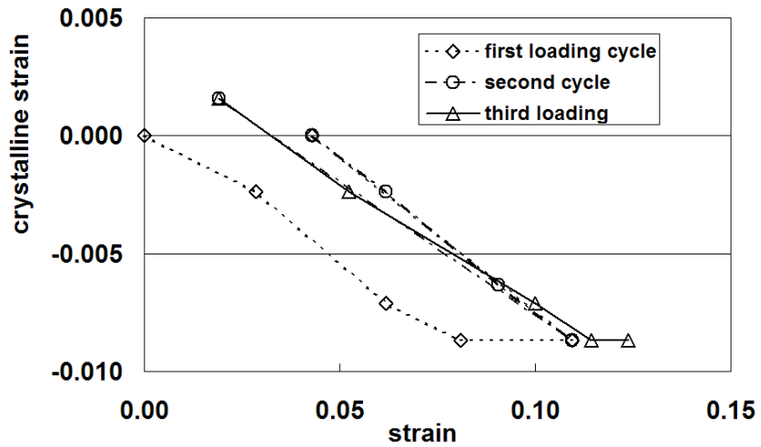

Fig. 4. Transversal crystalline strain vs. optically measured tensile strain of semi-crystalline iPP specimen estimated via the shift of the (1 1 0)-reflex at room temperature.

In a range of up to about 8 % strain the crystallites deform transversally by about -0.8 %. The mismatch between crystalline and global strain indicates the different stiffness of the crystallites compared to the whole specimen due to the relatively soft amorphous regions. During further loading the strain of the crystallites remains constant. This means that further deformation is realised on the micro-scale only by the amorphous phase and by additional shear dislocation of the crystallites.

4.4 Crystallite orientation of the samples and reorientation during drawing

In a preliminary investigation at BW4 stepwise loading at different temperature was performed. The stress-strain-diagrams captured during these measurements are presented in detail recently (Schneider, 2010, 2011), they are comparable to the mechanical behaviour of the preliminary tests. The stress-strain-level is slightly lower due to the generally lower strain rate. For the flat samples under investigation the transmission was 0.83 in the unstretched state. During stretching and simultaneous thinning the transmission generally increased to 0.96.

The images were always transformed to reference coordinate systems with respect to the scattering angles (scattering angle 2Θ and azimuthal angle φ or scattering vectors s_{12} and s_3). For further discussion the scattering intensity was projected over a selected range of φ on the 2Θ-axis. Figure 5 shows some characteristic equatorial cuts together with the transformed pattern.

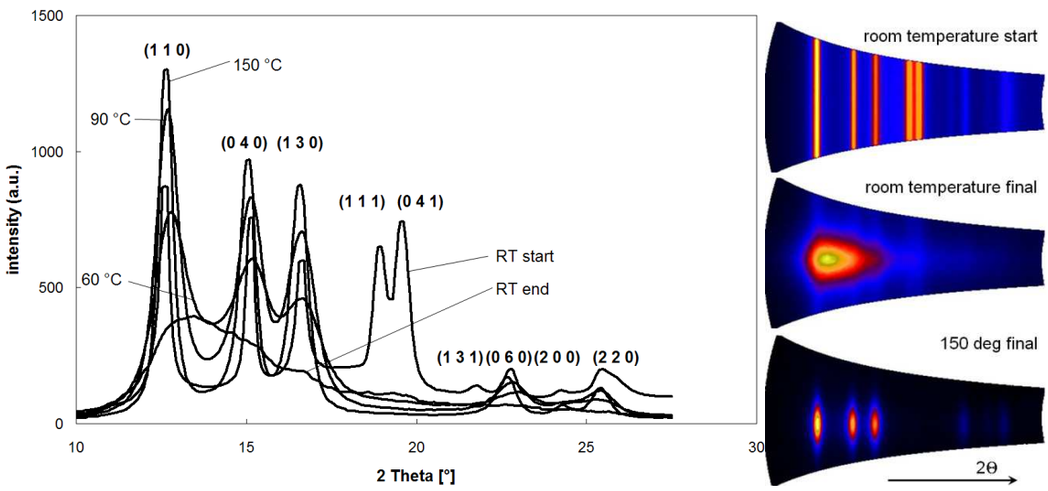

Fig. 5. Equatorial scattering intensity of undeformed iPP at room temperature and during strain hardening at elevated temperatures. The curves always show a projection of the angular range of ±2 ° around the equatorial direction. Right: WAXS-patterns, azimuthal angle vs. scattering angle 2Θ at three characteristic points: undeformed as well as immediately before failure at room temperature and 150 °C.

During deformation the WAXS patterns change in a quite characteristic way, see figure 6. Initially the intensity of the crystalline peaks is relatively constant over the azimuthal angle pointing to a homogeneous distribution of crystallite directions. At deformations below the yield point slight changes in the intensity of the peaks are reversible.

Above the yield point the deformation behaviour is strongly temperature-dependent. Generally in the investigated equatorial direction only the (h k 0)-peaks remain and the scattering intensity concentrates azimuthally in equatorial direction. This is generally an indication of orientation of crystallites with the c-axis (chain direction) in tensile direction. But while the peaks sharpen with increasing temperature, which is an indication of growing crystallites, they decrease strongly and broaden at temperatures in the range immediately above room temperature. This indicates a gradual disruption of crystallites into smaller fragments. Finally, at room temperature the distinct peaks disappear but give a broad halo in the angular range of the previous peaks. This indicates a rough orientation of the chains or very small crystallite fragments in tensile direction, probably in the form of fibrils. However, the thermal mobility of the chains seems to be all in all insufficient to establish new crystallites.

After these recent investigations with simultaneous SAXS and WAXS measurements with limited range of the WAXS-detector (Schneider, 2010) some representative WAXS measurements were repeated at elevated temperatures with whole WAXS-range and certain temperature-strain-program. The samples were heated to 110 °C in the tensile rig. At this temperature the samples were stretched to about 300 %. Afterwards they were heated

stepwise to temperatures below the melting temperature and cooled again up to 80 °C, both with and without load. The individual behaviour is described in detail.

The investigated injection moulded samples showed initially mostly homogeneous WAXS pattern with Debye-Scherrer patterns related to the reflexes mentioned in table 1. The samples are to a large extent crystallised. Heating the samples to about 110 °C didn't change the WAXS pattern.

During stretching the samples to about 300 % the pattern changed drastically, see figure 6. The intensity of the rings concentrates to certain positions, characteristic for well aligned crystallites in stretching direction.

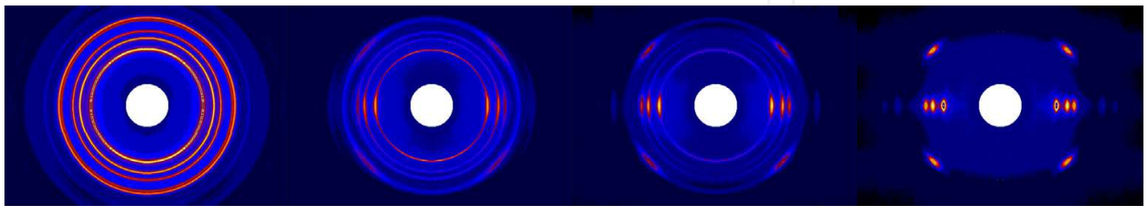

Fig. 6. Changing of the WAXS pattern during deformation at 110 °C (strain from left to right: 0 %, 70 %, 85 %, 300 %) of a waisted specimen (mini-dumbbell). The stretching direction is vertical.

Under the condition of fibre symmetry signals in the pattern vertical to the tensile direction report highly oriented lamellae or lamellar fragments in tensile direction. This final pattern remains mainly constant also during further heating to about 160 °C (below the melting point) under load as well as unloaded.

Further heating of the samples very close to the melting point creates a sharpening and broadening of the crystalline reflexes in azimuthal direction: Apparently the thermal stress is released, the mobility of the unloaded crystallites becomes higher and the orientation of it becomes a little bit less, see figure 7.

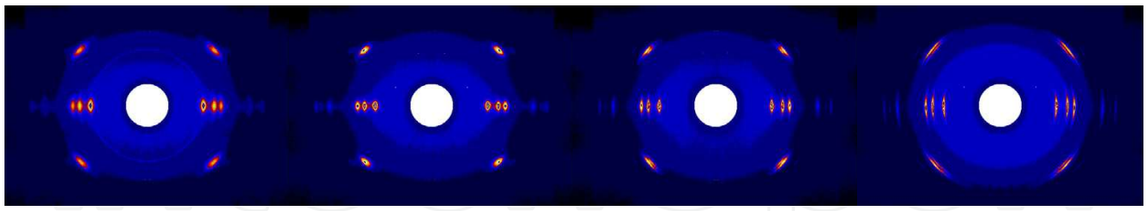

Fig. 7. Sharpening of the WAXS reflexes during deformation approaching the melting point (temperature from left to right: 110, 160, 165, 170 °C) of a waisted specimen (mini-dumbbell). The stretching direction is vertical.

Immediately above the last position in figure 7 the sample melts and all WAXS-reflexes disappear.

4.5 Crystallisation behaviour during subsequent cooling

The azimuthal width of the standard reflexes of the stretched iPP – if present - remains mainly constant also during following crystallisation processes by cooling. Cooling to about

140 °C doesn't change the pattern. During further cooling different routes of crystallisation can be observed, see figure 8.

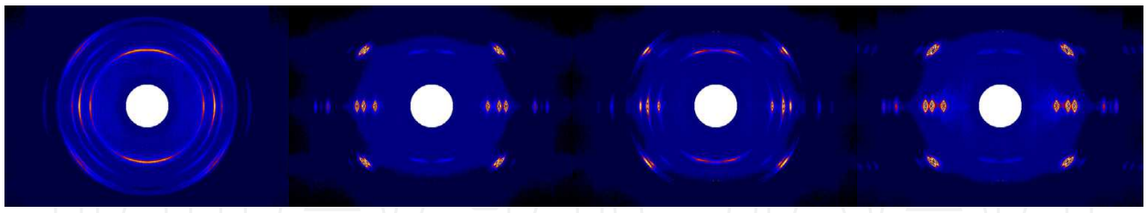

Fig. 8. Pattern during recrystallisation of a stretched iPP sample at temperatures below 140 °C: Isotropic pattern after crystallisation from the melt, a slight preferential orientation may be observed (creation of crystallites with a wide range of orientation); crystallisation of the common stretched lamellar fragments; generation of a meridional double-reflex (daughter lamellae); creation of a new series of (h k 1)-crystallites (from left to right). The stretching direction is vertical.

While the generally present reflexes of the lamellar fragments remain nearly unchanged, notable is the formation of a new meridional double-reflex with different strength. This reflex is discussed in the literature often as the formation of epitactic daughter lamellae (Kumaraswamy, 2000). Otherwise in some cases a whole system of reflexes in the plane of the (h k 1)-reflexes is found, which is described in the literature as nano-oriented crystals (Okada, 2010). The appearance of the latter depends strongly on a small temperature window below the melting point, to which the stretched sample must be heated.

4.6 Structural changes across a sample – influence of a temperature gradient

In the present investigations there had been a certain temperature gradient across the samples. So the initial temperature of the sample before cooling was different across the sample. As a consequence finally all the different structures discussed above could be found side by side in the same sample.

4.7 SAXS during stretching

From the set of successive scattering patterns during the deformation for the following discussion only patterns and the corresponding CDF's were chosen where characteristic changes could be seen.

The respective results of SAXS from stretching at room temperature are shown in figure 9. The regular circular form of the CDF from the beginning is nearly unchanged to about 6 % strain also during unloading. It represents the randomly distributed crystallites, which were deformed elastically, as discussed in the section about WAXS above. The diameter of the inner ring in the CDF indicates a lamellar thickness of 9.8 nm. The isotropic ring in the negative direction represents the long period of 17.7 nm. The following second positive and negative reflexes indicate a certain correlation with the third neighbours. Missing higher-order reflexes indicate that there are surprisingly no remarkable correlations above the third neighbours. During deformation below the yield point (loading, unloading, relaxation and repeated loading) this general situation is unchanged.

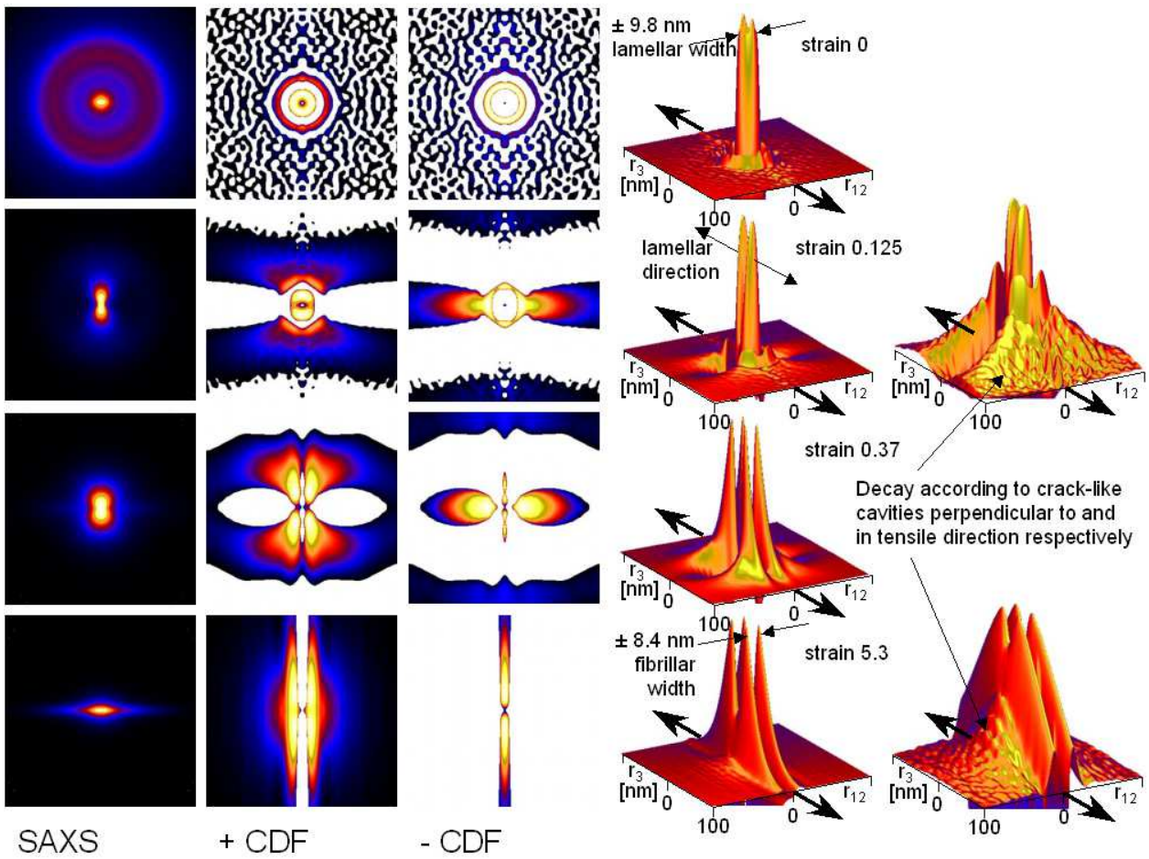

Fig. 9. Deformation of iPP at room temperature, from left to right: SAXS patterns, positive and negative CDF's (always log scale, pseudo-colour) as well as a surface plot of the CDF's (linear scale and for two strains also log scale) at different strains ε = 0.0, 0.125, 0.37 and 5.3 (from top). Each square of the pattern covers a range – 0.12 nm^{-1} < s_1, s_3 < 0.12 nm^{-1}, each square of the 2D-CDF covers a range of – 100 nm < r_{12}, r_3 < 100 nm, fibre direction always vertical. The stretching (fibre) direction is indicated in the surface plots by arrows.

Beyond the yield point the situation changes drastically. First of all it is noticeable that the total scattering intensity as well as the extrapolated intensity I_0 increase dramatically suggesting the activity of new strong scatterers – presumably cavities, which exhibit a strong scattering contrast to iPP due to their extremely low electron density. They start as small cracks transversal to the tensile direction and finally deform to long drawn cavities between fibrils. According to their successive growth and hence their broadly distributed dimensions they hardly show distinct scattering signals, but overlap with the signals arising from the lamellae or their fragments. The growing cavities are also responsible for the whitening of the cold drawn samples (see also Pawlak, 2010). In contrast to the scanning experiments with a microbeam reported by Roth (Roth, 2003), which allows to resolve certain individual voids, here over a large ensemble of cavities is averaged. Within the CDF's these cavities are reflected by the broad initial decay in fibre direction, at higher strains perpendicular to fibre direction, see figure 9, CDF's in log scale on the right.

Yet at a strain of 12.5 %, the beginning of the yielding region, the structure becomes anisotropic. While thickness of the lamellae remains constant, they align perpendicular to

the tensile direction. The correlation to the next neighbours in transversal direction is lost and concentrated within a 4-point-pattern. This indicates occasionally an internal shear deformation. Under the external stress the lamellae are sheared and finally break down into certain blocks as described by Strobl (Hong, 2004).

A new transversal correlation length is established at about 37 % strain. By shearing the lamellar blocks break down to a size which later represents the dimensions of the fibrils. According to the relatively low internal mobility the aligned chains are not able to form new crystallites. Their mean dimension in transversal direction is with 8.4 nm clearly below the lamellar thickness. This correlates with the WAXS results, which also indicate the final disappearance of the lamellar transversal order during cold drawing. Ultimately, at high strains, this transversal correlation dominates the whole CDF.

The general changes within the oriented chains – within crystallites as well as non-crystallized stretched chains – are shown in the sketch in figure 10, deformation at room temperature is shown in steps a), b), c), f) and g).

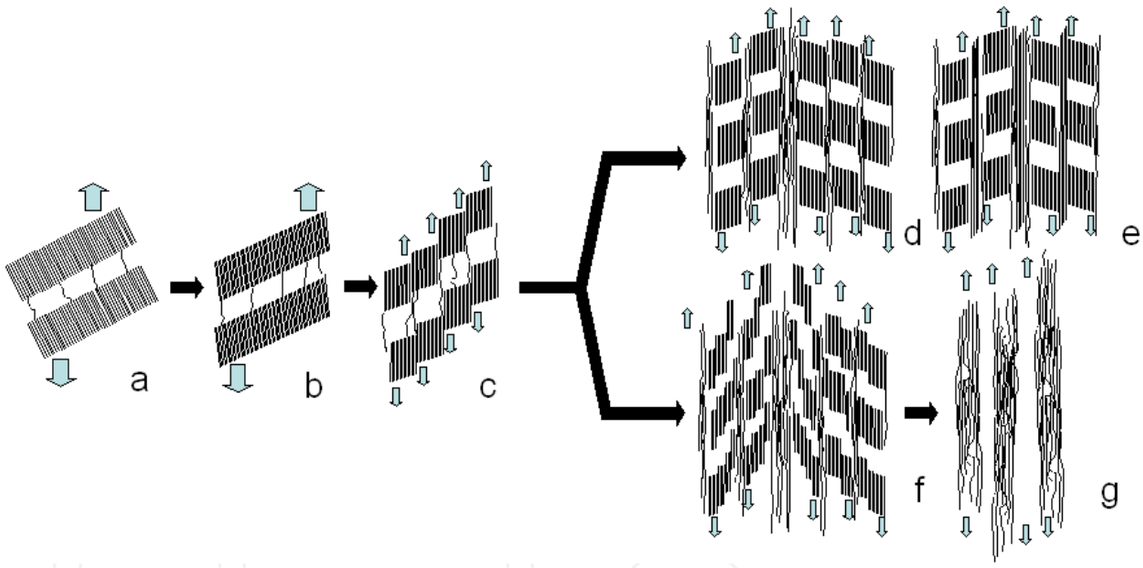

Fig. 10. Sketch of the transformations of the oriented chains during deformation, in-between are additional amorphous chains: a) lamellae with some tie-molecules, b) elastic shear-deformation of lamellae under small load and reorientation with respect to the load, c) fracture of lamellae into smaller blocks due to local stress concentration caused by tie molecules, d) stretched aligned, but not re-crystallised chains between the blocks during stretching at higher temperatures, e) some of the fibrillar arranged molecules crystallise, final stage in the case of hot stretched iPP, f) further dissolution of the blocks creating more extended chains at room temperature, g) finally, there are several strands of extended chains, not crystallised, with some amorphous regions in between, final stage in the case of cold stretched iPP.

With increasing temperature the deformation behaviour totally changes. The patterns and the CDF's of the stretching of iPP at 130 °C are shown in figure 11. Here the averaged as well as the extrapolated maximum intensity I_0 does not change dramatically above the yield

point. Instead soon the lamellae align in tensile direction increasing their correlation in this direction, indicated by higher order of reflexes in the CDF's. The transversal displacement of the reflexes suggests that the aligned lamellae are shifted against each other. The situation does not change generally also at high strains. This interpretation is also supported by the WAXS results described above. The deformation is shown schematically in figure 10 a) – e).

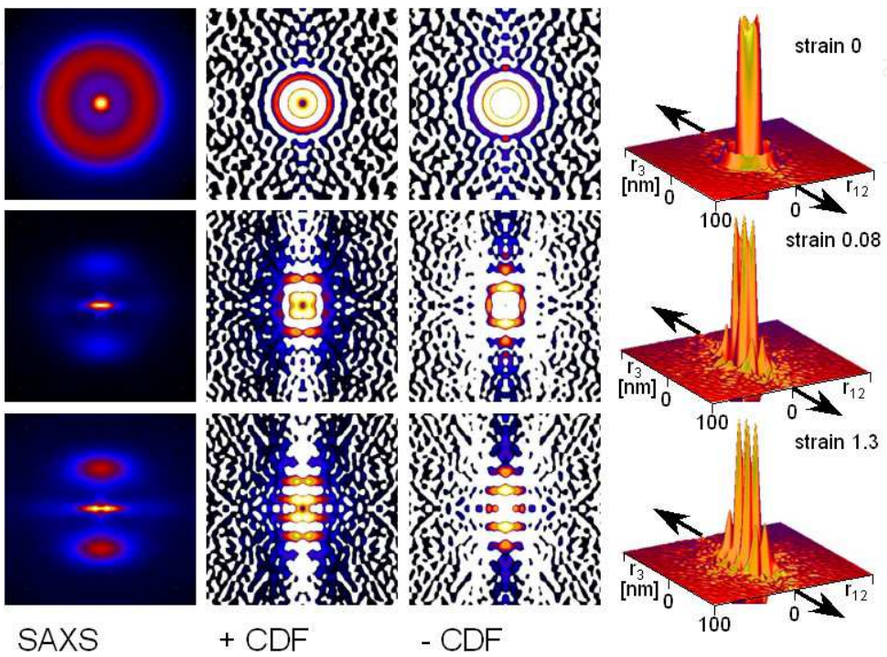

Fig. 11. Deformation of iPP at at 130 °C, from left to right: SAXS patterns, positive and negative CDF's (always log scale, pseudo-colour) as well as a surface plot of the CDF's (linear scale) at different strains ε = 0.0, 0.08 and 1.3 (from top). Each square of the pattern covers a range – 0.12 nm^{-1} < s_1, s_3 < 0.12 nm^{-1}, each square of the 2D-CDF covers a range of -100 nm < r_{12}, r_3 < 100 nm, fibre direction always vertical. The stretching (fibre) direction is indicated in the surface plot by arrows.

With increasing temperature also the whitening is remarkably reduced indicating that due to the higher mobility of the amorphous phase nearly cavitation is negligible as compared to the extent observed at room temperature.

Over the whole deformation range stress relaxation is observed as soon as the tensile rig was stopped. However since this can be ascribed to the amorphous phase, SAXS results remain mostly unaffected.

4.8 Influence of processing on the samples morphology

The influence of injection moulding on a preliminary orientation of the crystallites and their deformation we described recently (Schneider, 2010). It was shown, that injection moulded specimens in injection direction as well as the compression moulded and quickly cooled specimens are highly stretchable. By contrast the specimens transversal to the injection direction fail very soon. Here in some cases even crazing could be observed before failure.

This points out that there will be a strong structural anisotropy due to the processing history (shear stress as well as cooling rate).

4.9 DSC investigation of unstretched and stretched specimens

To check the thermal behaviour respectively melting of different stretched samples some DSC measurements were performed. In a first test samples were pre-stretched at different temperatures to about 500 %. The heating peaks of the first heating curves of the stretched samples are shown in fig. 12.

It seems to be possible to split each curve into 2 individual melting peaks whose positions shift with the stretching temperature to higher values. Furthermore, while the high-temperature peak is nearly constant the low-temperature peak increases with stretching temperature.

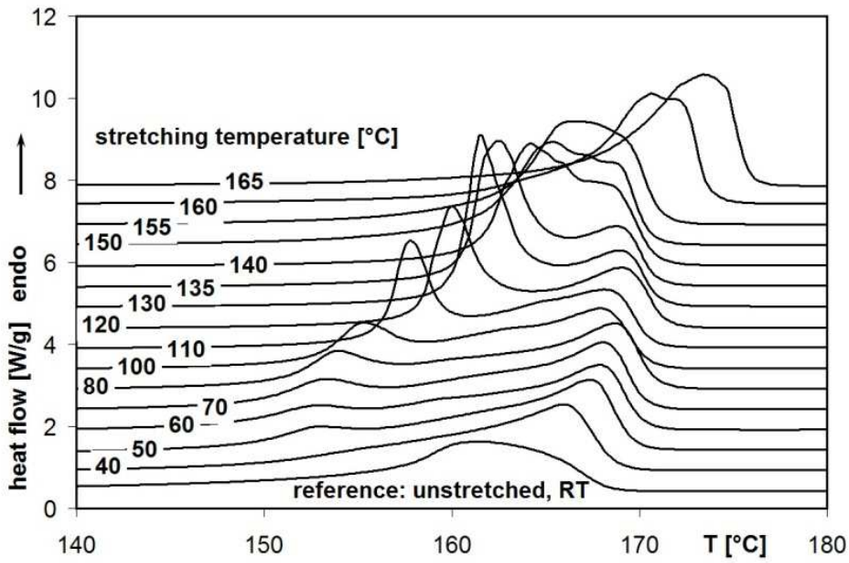

Fig. 12. DSC-measurements: first heating curves of compression moulded iPP-specimens stretched at different temperatures. For clarification the curves are vertically shifted.

To check, whether there are two individually melting crystalline species in a second series samples, stretched to about 500 % at 110 °C, were heated to different temperatures behind the first peak in the heating curve. Afterwards they were cooled to room temperature before they were heated over the melting point in a second run, see figure 13.

The position of the first peak flutters a little bit due to the different specimen taken from a stretched sample. Heating in the first run well above the melting temperature – 175 or 200 C – the second heating curve is similar to the first one with a slight double peak. If the first heating is stopped at 160 °C, the second heating curve has the narrower double peak, shifted to higher temperatures. Surprisingly in the case of the interrupted first heating at 165 °C the second heating peak is shifted to remarkable higher values and only a unique peak is observed.

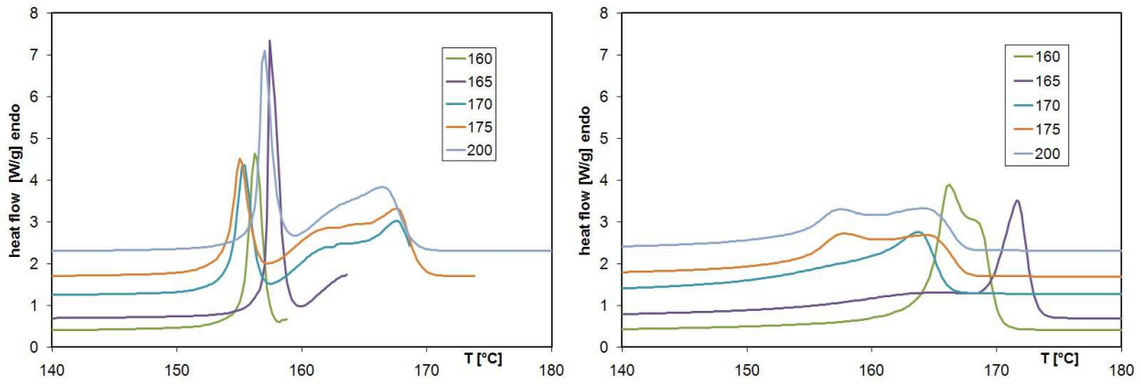

Fig. 13. DSC-measurements: first and second heating curves of compression moulded iPP-specimens stretched at 110 °C to about 500 %. The first heating was stopped at different temperatures after the first peak in the heating curve, see the label within the diagram. For clarification the curves are vertically shifted.

4.10 DMA investigation of unstretched and stretched specimens

The general different interaction of amorphous and crystalline regions in the initial (spherulitic) as well the highly stretched (fibrillar) state was investigated with DMA. The stretched material was produced by hot-stretching of small tensile samples from plates with a thickness of 4 mm and 10 mm width at different temperatures.

With shear and tensile load two independent measurements were performed, see figure 14. Under shear load the crystallites (fibrils) and the amorphous regions are more or less in series, under tensile load they are parallel. Accordingly the combination of the moduli is quite different.

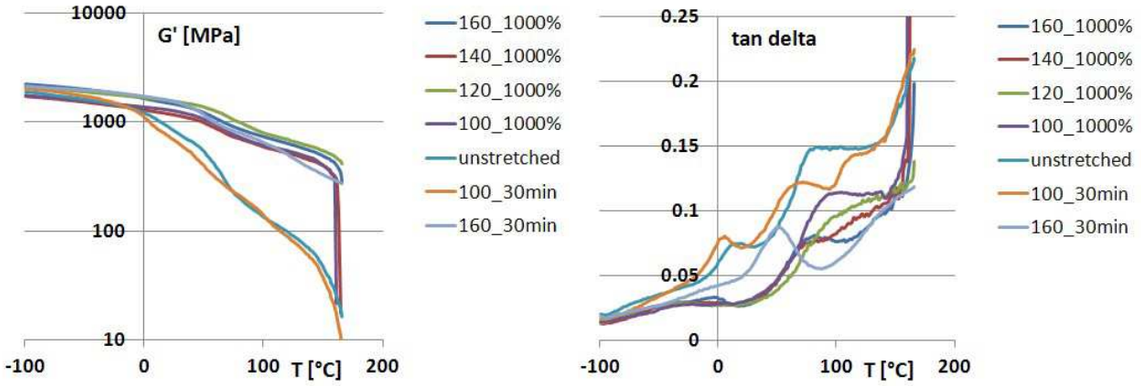

Fig. 14. Measurement under torsion: G′ (storage modulus) and loss tangent of differently treated iPP: injection moulded, annealed and hot-stretched samples. Parameters of the sample preparation are shown in the legend

At low temperatures the storage modulus is almost the same: Crystalline as well as amorphous regions behave stiff. At the common glass transition temperature at about 0 °C there is a small peak in the loss tangent and a decrease in the storage modulus due to the

onset of the mobility of the amorphous regions of the unstretched (annealed or not annealed) sample. This content is nearly missing in the case of the stretched samples.

In the range between room temperature and melting temperature there is a continuous drop in the storage modulus of the unstretched samples due to the increasing mobility of the amorphous phase with temperature. The amorphous phase is constrained between the crystalline one. Therefore, here is such a high temperature dependence of the mobility. Annealing at 100 °C enables some post- or re-crystallisation causing an increase in modulus and a decrease in the loss-tan. Annealing at 160 °C, i.e. shortly below the melting point, supports the further crystallization. The relatively strong drop down of G' remains.

The situation is totally different after high stretching. The signal of the undisturbed amorphous phase nearly totally disappears; the constrained amorphous phase enables only very slight molecular motion between the aligned crystallites. Annealing at increasing temperatures reduces this remaining mobility.

The behaviour under tensile load is somewhat different, see figure 15.

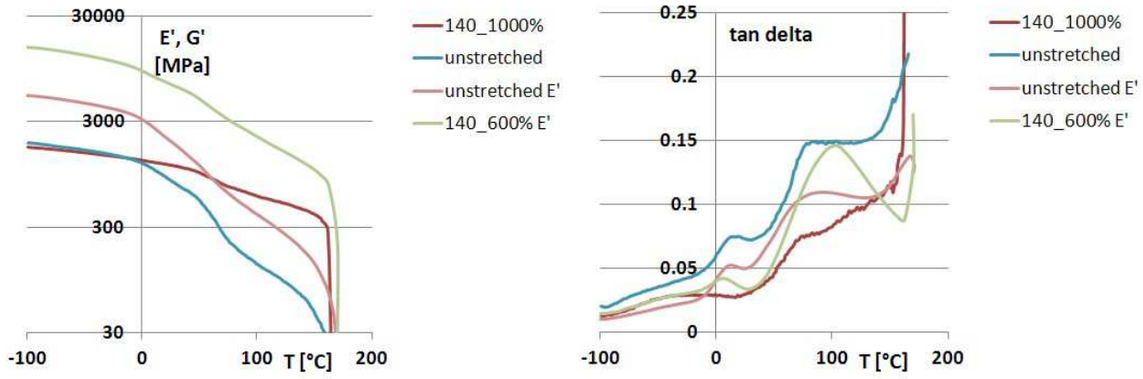

Fig. 15. Measurement under tension: E' (storage modulus) and loss tangent of differently treated iPP in comparison to the torsion measurement G': injection moulded and hot-stretched

Besides the generally higher values of the tensile modulus with respect to the shear modulus according to $E = 2 (1 + \mu) * G$, the crystalline and the amorphous phase after the stretching are more or less parallel. By this a noticeable increase in E', small contribution of the glass transition near 0 °C and a further softening around 100 °C appears.

4.11 Micrographs and SEM of stretched specimens

Micrographs under polarized light of iPP crystallised within a rheometer as well a stretched sample are shown in figure 16. Here the change from spherulitic to fibrillar structure is clearly visible. SEM images were taken to verify the described general deformation behaviour. Figures 17 to 20 show the compression moulded unstretched reference specimens and specimens stretched at room temperature, 90 °C and 150 °C. The specimens were cut in tensile direction, and vapour deposited with platinum. Stretching direction and thus s_3-axis are always vertical in the figures 17 to 20, the s_1-axis horizontal.

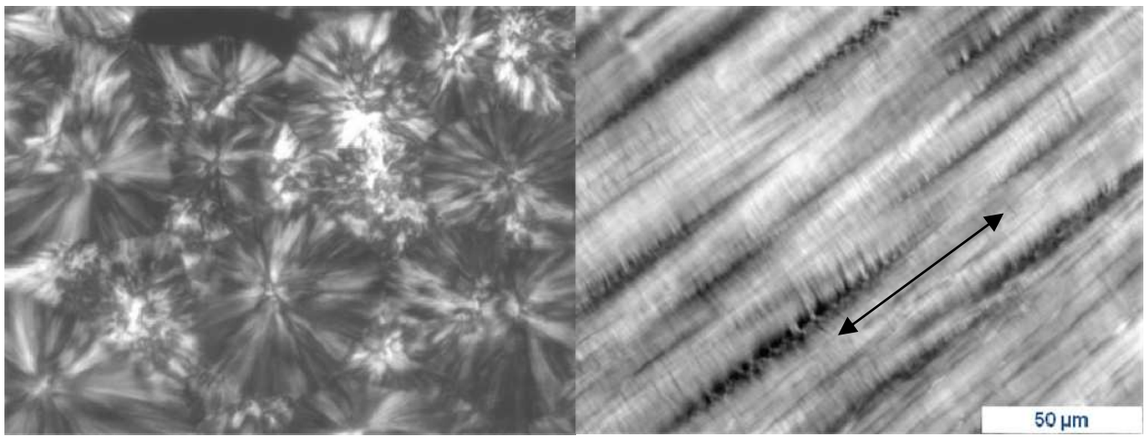

Fig. 16. iPP crystallised within a rheometer without shear and cold stretched sample with fibrillar strands (stretching direction diagonal, see arrow)

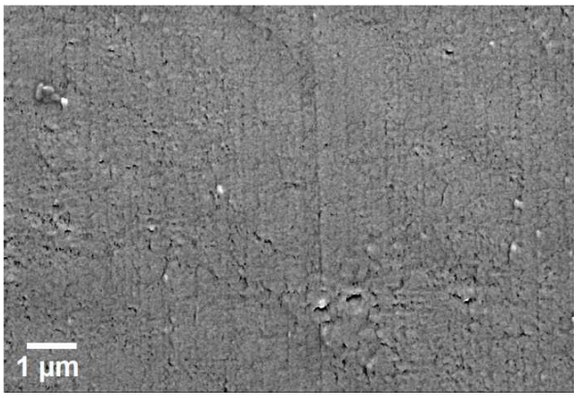

Fig. 17. Scanning electron micrograph of the unstretched reference iPP sample.

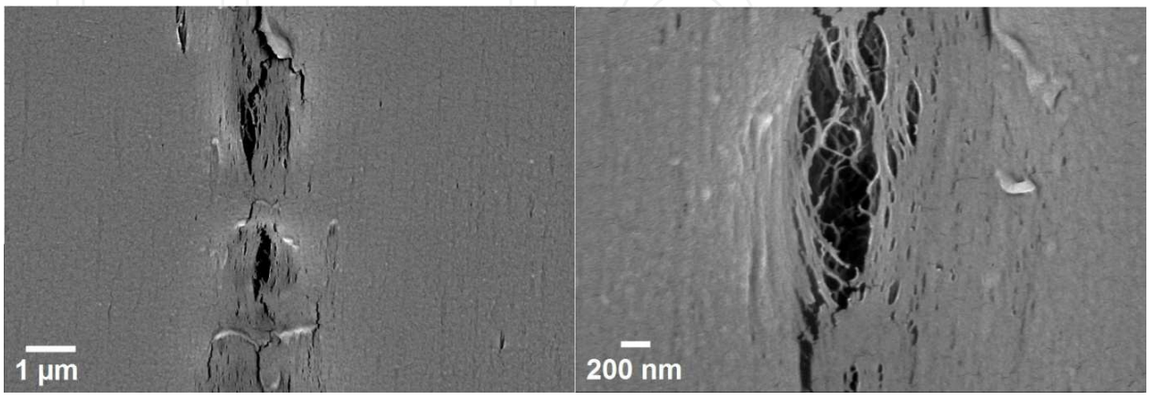

Fig. 18. Scanning electron micrograph of the iPP sample stretched at room temperature. Stretching direction vertical.

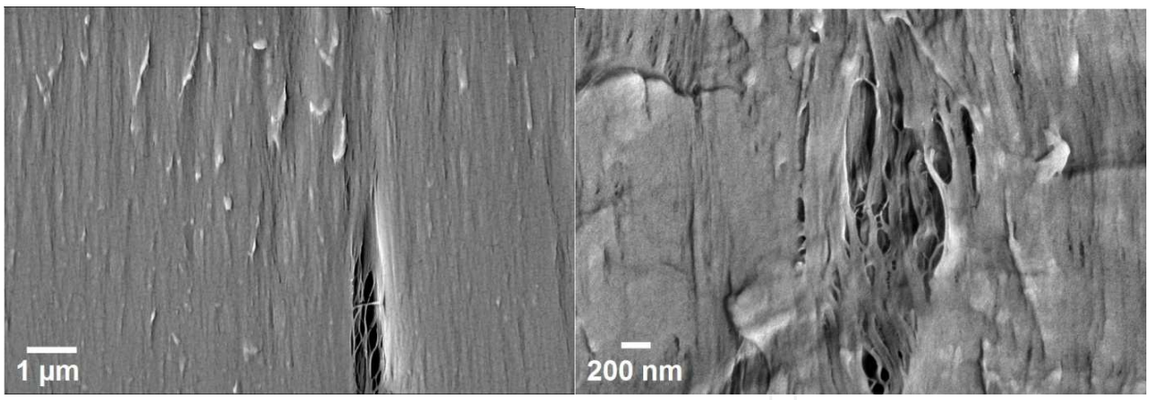

Fig. 19. Scanning electron micrograph of the iPP sample stretched at 90 °C. Stretching direction vertical

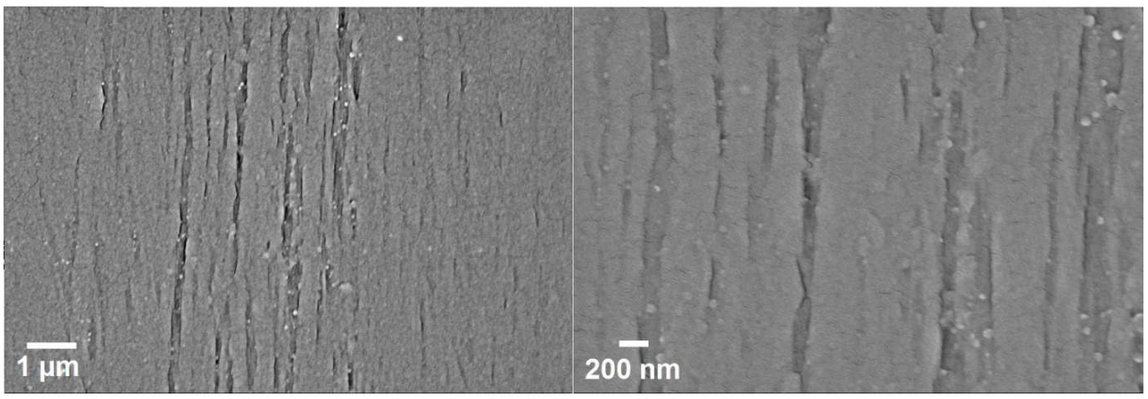

Fig. 20. Scanning electron micrograph of the iPP sample stretched at 150 °C. Stretching direction vertical.

Figure 17 to 20 show the voids in the stretched samples the formation of which was discussed above. Their size decreases with increasing stretching temperature. In the sample stretched at 150 °C they are not found. The lamellae and fibrillae are not visible at the present magnification, only a slight texture in stretching direction can be seen. A similar trend was reported recently by Pawlak (Pawlak, 2010), who found voids only at stretching temperatures below 60 °C, at higher temperatures only deformed spherulites and fibrils.

5. Discussion

Stretching semi-crystalline iPP at temperatures changes the morphology totally. Below about 80 °C the crystallites become destroyed, the stretched fragments oriented in stretching direction. This causes the wide peak in the WAXS pattern without a fine structure referring to the individual crystalline parameters. A strong cavitation appears because the transversal strength of the lamellae is less than that of the stretched amorphous phase, which one transfers stress to the lamellae. The relatively stiff but irregularized structure fails at comparable low stresses.

Stretching above about 80 °C causes a destruction of the initial morphology without cavitation. The crystalline/lamellar fragments were oriented via the stress transferred by the

tie molecules in stretching direction. Due to the high degree of crystallinity and mainly the transferred stress the amorphous regions between the oriented crystallites are in confined geometry and stretched. The stress of the amorphous phase is in balance to a load of the crystallites, which are slightly deformed on this way. The total degree of crystallinity changes only marginal. The frozen stresses can relax only approaching the melting temperature. There also the load of the crystallites goes down and the orientation in stretching direction becomes worse.

By aligning of crystallites or lamellar fragments by stretching as nuclei for subsequent crystallisation the whole morphology of a later fully crystallised material can become highly oriented. By this way the mechanical properties can become strongly improved. The accessible orientation by shearing a melt during processing is much lower than this route. This procedure to improve mechanical properties is normally used in hot drawing of melt spun fibres. But the present investigations show, that it should also be possible for macroscopic respectively 3-dimensional structures. It is much easier than the compression procedures of undercooled melt to get highly oriented material (Okada, 2010). The process is strongly dependent on the temperature regime. In the case of too strong heating all crystallites can melt and the sample will crystallise later on in a spherulitic or in the presence of nucleating agents and with sufficient quick cooling in an unoriented manner.

The splitting of the melting peak of stretched iPP seems to be initially due to the frozen internal stresses. The first peak appears if the stresses are finally released. This is, dependent on the stretching temperature, between 150 and 165 °C. The second heating shows again a double melting peak between 165 and 173 °C. The first part is due to the remaining lamellar fragments, the second due to the new established fibrils. If the first heating was to 165 °C, only a unique melting peak of the fibrils above 170 °C is found. It seems that this is also the region where the multitude of new crystalline reflexes is observed. This discussion of the material behaviour corrects our first conclusions about the melting behaviour of the different phases in stretched iPP, which we published recently (Schneider, 2010).

To describe the temperature-dependent stress-strain behaviour of semi-crystalline materials we established a model on the basis of the described structural elements. It describes the interaction of the temperature-dependent mobility of the amorphous phase, the initially relative stable crystalline phase, the step-wise re-arrangement of the crystalline phase with respect to orientation and transformation via crystallite fragments and extended chains into fibrils. It will be soon published separately.

6. Conclusion

The experiments revealed the continuously changing interplay of elastic and plastic deformation and energy dissipation (the transformations of amorphous and crystalline phases) during deformation of semi-crystalline polymers using the example of iPP. Due to the high number of parallel processes, here the use of structure characterisation by X-ray scattering techniques was used in small and wide angle range and complemented by mechanical tests, DMA, DSC and SEM. The combination of these methods is likely to provide a well-founded basis for understanding material structure. DSC is an essential extension to characterise crystallisation behaviour.

It was found that there is a strong temperature-dependent interaction of deformations within the amorphous phase and reorientations as well as transformations of crystalline units. They are strongly determined by the molecular structure as well as the processing-dependent initial morphology of the samples. According to the temperature-dependent mobility within the amorphous phase the stress transfer to the crystalline phase and so the changes within this phase are also strongly temperature-dependent.

On the other side by re-melting, stretching and re-crystallizing semi-crystalline material it is possible to get materials with highly improved mechanical behaviour due to well-defined and strongly oriented re-crystallisation. Of cause for using this general technique the parameters of treatment must be optimized.

The mechanisms found and discussed here in the case of iPP seem to be very universal. It might also apply to other polymers. This will be checked in the future by additional investigations.

The detailed understanding of the multiple deformation and structure-establishing processes is an essential base for the development of semi-crystalline materials with well-defined properties.

7. Acknowledgement

The authors are grateful to HASYLAB for beamtime within the projects II-20060086 and I-20100280 and A. Timmann, J. Perlich and M. A. Kashem for local support, and N. Stribeck (University of Hamburg) for the support in the course of data evaluation. They thank their colleagues from the IPF for support, in particular V. Körber for the construction of the tensile rig, W. Jenschke for the software support for the tensile rig, R. Boldt for SEM micrographs, R. Vogel and R. Jurk for DMA-measurements, and D. Krause for sample preparation.

8. References

Breese, D.R. & Beaucage, G. (2004). A review of modeling approaches for oriented semi-crystalline polymers, *Current Opinion in Solid State and Materials Science*, Vol. 8 (2004), pp. 439-448

Breese, D.R. & Beaucage, G. (2008). Modeling the mechanical properties of highly oriented polymer films: A fiber/gel composite theory approach, *Journal of Polymer Science: Part B: Polymer Physics*, Vol. 46, No. 6 (2008), pp. 607-618

Davies, R. J. et al. (2004). The use of Synchrotron X-ray Scattering coupled with in situ Mechanical Testing for studying Deformation and Structural change in Isotactic Polypropylene, *Colloid. Polym. Sci.,* Vol. 282 (2004), pp.854-866

Gehrke, R. et al. (1995). An ultrasmall angle scattering instrument for the DORIS-III bypass, *Rev. Sci. Instrum.* Vol. 66 (1995), pp. 1354-1356

Gibson, A.G. at al. (1978). Dynamic mechanical behaviour and longitudinal crystal thickness measurements on ultra-high modulus linear polyethylene: a quantitative model for the elastic modulus, *Polymer,* Vol. 19 (1978), pp. 683-693

Hong, K. et al. (2004). A model treating tensile deformation of semi-crystalline polymers: Quasi-static stress-strain relationship and viscous stress determined for a sample of

polyethylene. *Macromolecules,* Vol. 37, 2004, pp.10165-73 and Model treatment of tensile deformation of semicrystalline polymers: Static elastic moduli and creep parameters derived for a sample of polyethylene, *Macromolecules,* Vol. 37 (2004), pp.19174-79

Hong, K. & Strobl, G. (2006). Network stretching during tensile drawing of polyethylene: A study using X-ray scattering and microscopy, *Macromolecules* Vol.39 (2006), pp.268-273

Kumaraswamy, G. et al. (2000). Shear-Enhanced Crystallization in Isotactic Polypropylene: 2. Analysis of the formation of the Oriented 'Skin', *Polymer* Vol.41 (2000), pp.8931-8940

Kurelec, L. et al. (2005). Strain hardening modulus as a measure of environmental stress crack resistance of high density polyethylene, *Polymer,* Vol. 46 (2005), pp. 6369-6379

Lode, U. et al. (1998). Development of crazes in polycarbonate, investigated by ultra small angle X-ray scattering of synchrotron radiation, *Macromol. Rapid Commun.* Vol. 19 (1998), pp.35-39

Men, Y.M. et al. (2004). Synchrotron Ultrasmall-Angle X-ray Scattering Studies on Tensile Deformation of Poly(1-butene), *Macromolecules* Vol. 37 (2004), pp. 9481-9488

Okada, K.N. et al. (2010). Elongational crystallization of isotactic polypropylene forms nano-oriented crystals with ultra-high performance, *Polymer Journal* Vol. 42 (2010), pp.464-473

Pawlak, A. & Galeski, A. (2010). Cavitation and morphological changes in polypropylene deformed at elevated temperatures, *Journal of Polymer Science: Part B: Polymer Physics* Vol.48 (2010), pp.1271-1280

Peterlin, A. (1971). Molecular model of drawing polyethylene and polypropylene, *J. Mat. Sci.* Vol.6 (1971), pp.490-508

Roth, S.V. et al. (2003). Fatigue behaviour of industrial polymers - a microbeam small-angle X-ray scattering investigation, *J. Appl. Cryst.* Vol.36 (2003), pp.684-688

Roth, S.V. et al. (2006). Small-angle options of the upgraded ultrasmall-angle x-ray scattering beamline BW4 at HASYLAB, *Rev. Sci. Instrum.* Vol.77 (2006), 085106

Roth, S.V. et al. (2011). In situ observation of cluster formation during nanoparticle solution casting on a colloidal film, *J. Phys. Condens. Matter* Vol. 23 (2011), 254208

Schneider, K. et al. (2006). The Study of Cavitation in HDPE Using Time Resolved Synchrotron X-ray Scattering During Tensile Deformation, *Macromolecular Symposia* Vol.236 (2006), 241-248

Schneider, K. & Schöne, A. (2008). Online-structure characterisation of polymers during deformation and relaxation by Synchrotron-SAXS and WAXS, In: *Reinforced Elastomers: Fracture Mechanics, Statistical Physics and Numerical Simulations*; Kaliske, M.; Heinrich, G. & Verron, E. (Eds.); EUROMECH Colloquium 502, Dresden, 2008 pp.79-81

Schneider, K. et al. (2009). Investigation of changes in crystalline and amorphous structure during deformation of nano-reinforced semi-crystalline polymers by space-resolved synchrotron SAXS and WAXS, *Procedia Engineering* Vol.1 (2009), pp.159-162

Schneider, K. (2010). Investigation of Structural Changes in Semi-Crystalline Polymers During Deformation by Synchrotron X-Ray Scattering, *Journal of Polymer Science: Part B: Polymer Physics,* Vol.48 (2010), pp.1574-1586

Schneider, K. et al. (2011). Online structure investigation during deformation and fracture using synchrotron radiation, *Proceedings of 13. Problemseminar "Deformation und Bruchverhalten von Kunststoffen"*, CD-ROM, ISBN 978-3-86829-400-2, Halle-Merseburg, 29.6.-1.7.2011, pp. 122-130

Schroer, C.G. et al. (2006). Mapping the local nanostructure inside a specimen by tomographic small-angle x-ray scattering, *Appl. Phys. Lett.* Vol.88 (2006), 164102

Stribeck, N. (2001). Extraction of domain structure information from small-angle X-ray patterns of bulk materials, *J. Appl. Cryst.* Vol.34 (2001), pp.496-503

Stribeck, N. (2007). *X-Ray Scattering of Soft Matter*, ISBN 978-3-540-69855-5, Springer. Heidelberg, 2007

Stribeck, N. et al. (2008). Nanostructure Evolution in Polypropylene During Mechanical Testing, *Macromol. Chem. Phys.* Vol. 209 (2008), pp.1992-2002

Vonk, C.G. (1979). A small angle X-ray scattering study of polyethylene fibres, using the two-dimensional correlation function, *Colloid Polym. Sci.* Vol. 257 (1979), pp.1021-1032

Weeks, N.E. & Porter, R.S. (1974). Mechanical properties of ultra-oriented polyethylene, *Journal of Polymer Science: Part B: Polymer Physics* Vol.12 (1974), pp.635-643

Zuo, F. et al. (2005). An in Situ X-ray Structural Study of Olefin Block and Random Copolymers under Uniaxial Deformation. *Macromolecules*, Vol. 38 (2005), 3883

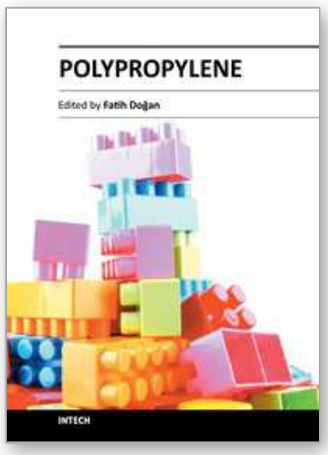

Polypropylene

Edited by Dr. Fatih Dogan

ISBN 978-953-51-0636-4

Hard cover, 500 pages

Publisher InTech

Published online 30, May, 2012

Published in print edition May, 2012

This book aims to bring together researchers and their papers on polypropylene, and to describe and illustrate the developmental stages polypropylene has gone through over the last 70 years. Besides, one can find papers not only on every application and practice of polypropylene but also on the latest polypropylene technologies. It is also intended in this compilation to present information on polypropylene in a medium readily accessible for any reader.

How to reference

In order to correctly reference this scholarly work, feel free to copy and paste the following:

K. Schneider, L. Häussler and S.V. Roth (2012). Tailoring of Morphology and Mechanical Properties of Isotactic Polypropylene by Processing, Polypropylene, Dr. Fatih Dogan (Ed.), ISBN: 978-953-51-0636-4, InTech, Available from: http://www.intechopen.com/books/polypropylene/tailoring-of-morphology-and-mechanical-properties-of-ipp-by-processing

INTECH
open science | open minds

InTech Europe
University Campus STeP Ri
Slavka Krautzeka 83/A
51000 Rijeka, Croatia
Phone: +385 (51) 770 447
Fax: +385 (51) 686 166
www.intechopen.com

InTech China
Unit 405, Office Block, Hotel Equatorial Shanghai
No.65, Yan An Road (West), Shanghai, 200040, China
中国上海市延安西路65号上海国际贵都大饭店办公楼405单元
Phone: +86-21-62489820
Fax: +86-21-62489821

IntechOpen